JOURNAL OF GEOPHYSICAL RESEARCH, VOL. 112, D24S31, doi:10.1029/2007JD008788, 2007

High Resolution Dynamics Limb Sounder observations of polar stratospheric clouds and subvisible cirrus

Steven Massie,[1] John Gille,[1] Rashid Khosravi,[1] Hyunah Lee,[1] Douglas Kinnison,[1] Gene Francis,[1] Bruno Nardi,[1] Thomas Eden,[1] Cheryl Craig,[1] Chris Halvorson,[1] Michael Coffey,[1] Daniel Packman,[1] Charles Cavanaugh,[1] James Craft,[2] Vincil Dean,[2] David Ellis,[2] John Barnett,[3] Christopher Hepplewhite,[3] Alyn Lambert,[4] Gloria Manney,[4,5] Anthony Strawa,[6] and Marion Legg[7]

Received 12 April 2007; revised 28 August 2007; accepted 12 September 2007; published 15 December 2007.

[1] The High Resolution Dynamics Limb Sounder (HIRDLS) cloud detection and cloud top determination algorithm is described and applied to 2005–2007 HIRDLS radiance profiles. Statistical averages of HIRDLS and correlative cloud data are highly correlated. The 1998–2005 Halogen Occultation Experiment (HALOE) and HIRDLS time averaged cloud top pressures have a correlation coefficient of 0.87 and 0.93 in the tropics and midlatitudes, respectively. Time series of the temperature T < 195 K hemispherical area, on the 450 K potential temperature surface, and the total number of polar stratospheric clouds observed by the HIRDLS experiment in January and February 2005 have a correlation coefficient of 0.92. HALOE and HIRDLS normalized distributions of cloud counts, expressed as a function of outgoing longwave radiation (OLR), have a correlation coefficient of 0.99. Tropical averages of 1998–2005 HALOE and HIRDLS cloud occurrence frequencies at 82 and 100 hPa are within 25% of each other, and the morphology of latitude-longitude contour maps of cloud frequency are similar. Colocated Stratospheric Aerosol and Gas Experiment (SAGE III) and HIRDLS cloud top pressure values in 2005 have a correlation coefficient of 0.85 when the distance between observations is less than 100 km and the time difference is less than 6 h. Correlations between colocated SAGE III and HIRDLS cloud top pressures improve as space and time differences decrease.

Citation: Massie, S., et al. (2007), High Resolution Dynamics Limb Sounder observations of polar stratospheric clouds and subvisible cirrus, *J. Geophys. Res.*, *112*, D24S31, doi:10.1029/2007JD008788.

1. Introduction

[2] Polar stratospheric clouds (PSCs), cirrus, and stratospheric aerosol are of interest because of their physical effects in the atmosphere. PSCs and cold sulfate particles are responsible for the heterogeneous chemistry that converts inactive chlorine into active chlorine in the polar stratosphere [*World Meteorological Organization*, 1999]. The manner in which "ozone hole" losses evolve in the coming decades is dependent upon the evolution of inactive chlorine concentrations, stratospheric temperatures, dynamics, and cold sulfate and PSC surface area. Monitoring of these field variables will be necessary to understand how the lower stratosphere evolves during the forthcoming decades. Cirrus near the tropopause plays an important role in the processes that dehydrate the upper troposphere and lower stratosphere (UT/LS) [*Jensen et al.*, 2001; *Jensen and Pfister*, 2004], and influence the radiative balance of the UT/LS [*Jensen et al.*, 1994]. The growth of cirrus particles sequesters water vapor, and the sedimentation of ice in rising air parcels slowly diminishes the water content, leading to a dry stratosphere. It is of interest to understand these coupled dynamical/microphysical processes, and to assess if these processes change with time this century because of possible changes in convective activity and tropospheric temperature. Finally, the stratospheric sulfate layer undergoes dramatic changes in mass loading following major volcanic episodes. The temperature changes associated with these major mass loadings have served as important tests of climate models [*Hansen et al.*, 2002; *Santer et al.*, 2003].

[3] Clouds and aerosols are also of interest because of their impact upon remotely sensed radiation fields. While molecular spectra can be readily calculated as a function of

[1]National Center for Atmospheric Research, Boulder, Colorado, USA.
[2]Center for Limb Atmospheric Sounding, University of Colorado, Boulder, Colorado, USA.
[3]Department of Physics, University of Oxford, Oxford, UK.
[4]Jet Propulsion Laboratory, California Institute of Technology, Pasadena, California, USA.
[5]Also at New Mexico Institute of Mining and Technology, Socorro, New Mexico, USA.
[6]NASA Ames Research Center, Moffett Field, California, USA.
[7]Bay Area Environmental Research Institute, Sonoma, California, USA.

0148-0227/07/2007JD008788$09.00

concentration, pressure, and temperature, aerosol spectra are not as well characterized. Many possible particle size distributions and compositions determine the wavelength dependencies of cloud and aerosol infrared extinction spectra. The addition of clouds and aerosol along a line of sight greatly increases the number of unknown variables that influence the wavelength-dependent radiation field of a remote sensing experiment.

[4] Clouds and aerosols have been studied for many decades by satellites. PSCs were first observed from space by the Stratospheric Aerosol Measurement (SAM II) solar occultation experiment [*McCormick et al.*, 1982]. Subsequent solar occultation experiments, including the Stratospheric Aerosol and Gas Experiment (SAGE) [*McCormick and Veiga*, 1992], Polar Ozone and Aerosol Measurement (POAM) [*Bevilacqua et al.*, 2002], and HALOE [*Russell et al.*, 1993] experiments, have measured stratospheric aerosol and PSCs from 1978 through 2005. Emission limb sensors, such as the Cryogenic Limb Array Etalon Spectrometer (CLAES) [*Roche et al.*, 1993] and Improved Stratospheric and Mesospheric Sounder (ISAMS) [*Taylor et al.*, 1993], measured PSCs in the early 1990s, while the Michelson Interferometer for Passive Atmospheric Sounding (MIPAS) is currently collecting PSC measurements [*Spang et al.*, 2005]. Measurements of cirrus near the tropopause commenced with SAGE [*Wang et al.*, 1996], and continued through 2005 with SAGE III [*Kent et al.*, 2007] and HALOE observations. Thin cirrus is commonly referred to as "subvisible" cirrus, since the human eye, looking upward, cannot detect these optically thin clouds. Cirrus extinctions near the tropopause were measured by CLAES [*Mergenthaler et al.*, 1999] from 1991 to 1993. With the recent launch of the Cloud-Aerosol Lidar and Infrared Pathfinder Satellite Observation (CALIPSO) satellite lidar in 2006, PSCs and tropopause cirrus are being measured from pole to pole at 532 nm and 1064 nm.

[5] HIRDLS (J. C. Gille et al., The High Resolution Dynamics Limb Sounder (HIRDLS): Experiment overview, results, and temperature validation, submitted to *Journal of Geophysical Research,* 2007, hereinafter referred to as Gille et al., submitted manuscript, 2007) joins the roster of space experiments which can measure clouds in the stratosphere and upper troposphere. HIRDLS is a limb viewing emission experiment with 21 spectral channels in the infrared, spanning the wavelength range from 6.2 to 17.2 μm, and was designed to measure temperature-pressure profiles, the mixing ratios of many gas species (i.e., O_3, HNO_3, H_2O, NO_2, N_2O, CH_4, CFC-11, CFC-12, $ClONO_2$, N_2O_5), and cloud/aerosol extinction profiles. HIRDLS obtains approximately 5500 profiles per day since a measurement sequence is carried out every 10 s, and covers the same latitude range from 67°S to 80°N each day.

[6] During the launch phase, however, Kapton insulation inside HIRDLS ruptured, and covers roughly 80% of the scan mirror assembly. Since the insulation radiates in the infrared, and is mechanically forced to oscillate by the scan mirror, the radiance field sensed by the 21 individual HIRDLS detectors is complicated. The insulation radiance dominates the total sensed signal. Much effort is being directed to account for this contamination, to accurately extract the atmospheric signal from the total radiation field, and to improve the retrievals of the impaired experiment.

[7] PSCs, tropopause cirrus, and deep convective clouds have large impacts upon atmospheric radiance profiles, especially in the HIRDLS 12.1 μm channel. The radiance R (w m^{-2} $ster^{-1}$) sensed by the HIRDLS emission experiment is governed by the equation

$$R = \int B \exp(-\tau) d\tau \quad (1)$$

where the total optical depth τ is the sum of gas τ_{gas}, cloud τ_{cloud}, and aerosol optical $\tau_{aerosol}$ depths, and B is the Planck function. Gas opacity in the 12.1 μm infrared "window channel" is very low, and the limb viewing geometry of the HIRDLS experiment leads to large τ_{cloud} values along a raypath. A tangent raypath has a ray segment ds of length ~300 km near the tangent ray point, so cloud extinction β (in km^{-1} units) along a limb viewing path produces an optical depth equal to β ds. PSC and subvisible cirrus extinctions in the infrared vary between 10^{-4} to 10^{-2} km^{-1}, yielding limb optical depths between 0.03 and 3. These large optical depths are larger than gas optical depths and enhance 12.1 μm atmospheric limb view radiances. Previous measurements of 12 μm PSC emission by ISAMS and CLAES [*Taylor et al.*, 1994; *Massie et al.*, 1994] and of subvisible cirrus by CLAES [*Mergenthaler et al.*, 1999] confirm this simple physics.

[8] Our paper is organized in the following manner. In section 2 we discuss how several cloud types are detected and identified in HIRDLS radiance profiles. Section 3 discusses how the operational retrieval is configured to solve for temperature-pressure, gas mixing ratio, and cloud/aerosol extinction profiles. Section 4 compares HALOE, SAGE III, and HIRDLS cloud top pressure measurements. HIRDLS PSC profile counting statistics and preliminary extinction measurements are discussed in section 5. HIRDLS tropical cloud detection characteristics and cloud frequency of occurrence latitude-longitude maps are compared to HALOE data in section 6. A common structural thread in this paper is (1) to illustrate that HIRDLS data can be used to detect (count) clouds in the stratosphere and troposphere, (2) to quantify how well HIRDLS cloud counting capability compares to other correlative data, and (3) to discuss the preliminary extinctions retrieved by the HIRDLS experiment. In section 7 we summarize our findings.

2. Cloud Detection

[9] Calibrated radiances in HIRDLS channel 6 (the 12.1 μm channel) are examined for the presence of clouds that perturb the radiance profile. Cloud detection processing on a given day is carried out using all radiance profiles only for the observation day of interest. The processing examines radiance profiles that are binned in latitude, since the shape of a radiance profile is influenced by the temperature profile. Latitude bins (e.g., 90–60°S, 60–30°S, 30°S–30°N, 30–60°N, 60–90°N) are selected to correspond to the latitude ranges of the polar, midlatitudes, and tropical regions. While the processing can be set up for a larger number of latitude bins, this decreases in an adverse manner the number of clear sky radiance profiles in each latitude bin. In general terms (specifics are discussed below), the

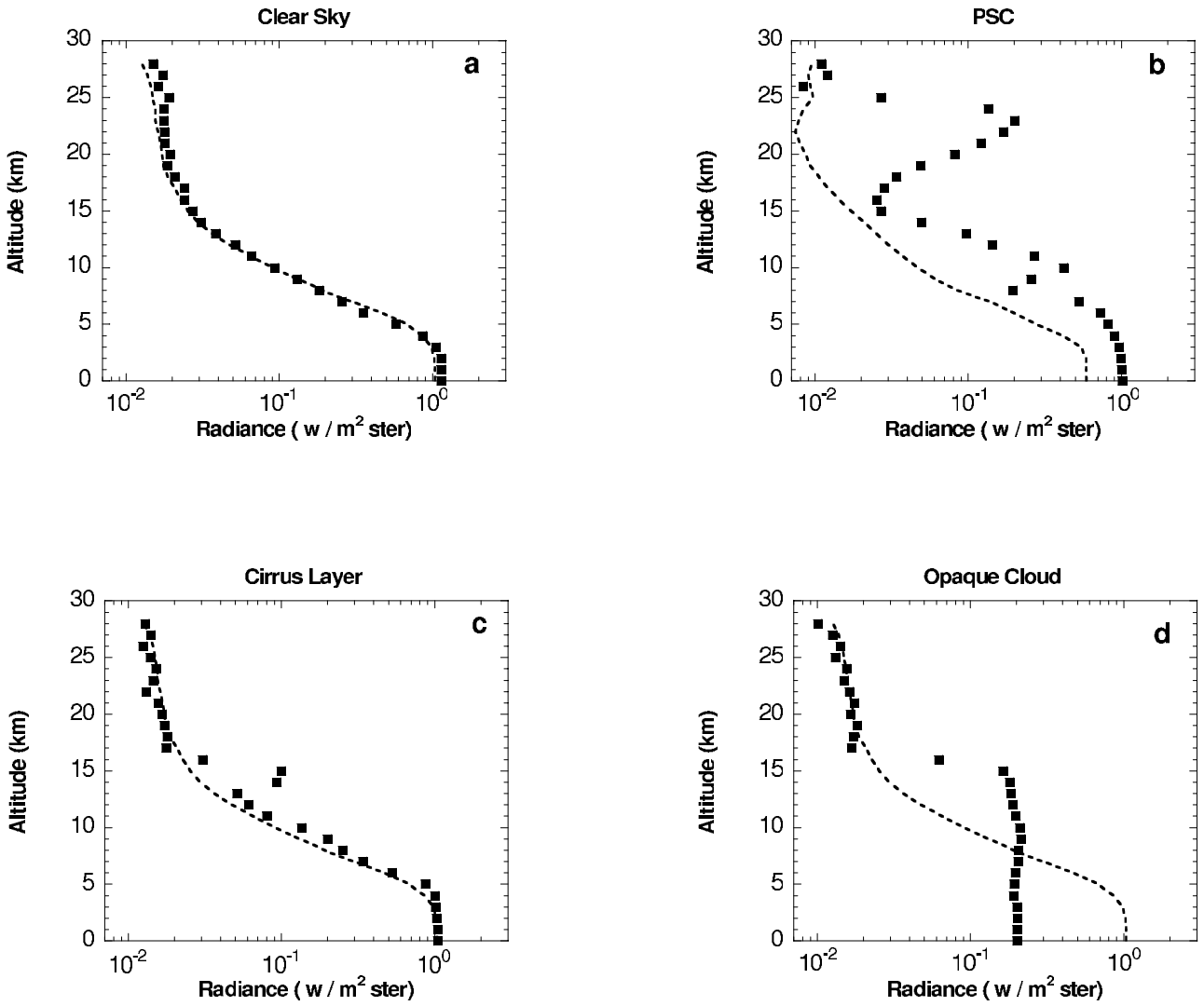

Figure 1. Four representative channel 6 (12.1 μm) radiance (single squares) and clear sky average profiles (dotted curves) on 27 January 2005, (a) clear sky (15.57°N, 216.20°E), (b) PSC (68.31°N, 343.41°E), (c) tropical cirrus layer (4.32°N, 220.00°E), and (d) opaque tropical cloud (16.79°S, 223.72°E) cases.

processing determines the average clear sky radiance profile for each latitude bin in an iterative manner. For the first iteration, all profiles are averaged, and standard deviations from the average are calculated. For the 2nd iteration, each profile is compared to the average profile (by techniques described in the following paragraph). If the profile is deemed to be influenced by clouds, then this profile is removed from the averaging process, and it is noted that this profile is cloud contaminated (and thus will not be used again to define the next iteration's average curve). The removal process is iterated five times. Once the final clear sky average radiance curve is determined, average curves are calculated for the other 20 HIRDLS spectral channels by averaging all profiles for which the channel 6 radiance profile did not have cloud contamination.

[10] Examples of cloud radiance perturbations are illustrated by the in-house v2.04.06 radiance profiles displayed in Figure 1. The clear sky average curve is given by the dashed line in all of the panels. As altitude increases, the noise characteristics of the radiance profile become evident (e.g., the jog in radiance at 25 km in Figure 1a of the tropical clear sky radiance profile is most likely not a cloud feature). Clouds, however, perturb the radiance profile in dramatic fashion. A PSC is seen in Figure 1b with a radiance peak near 23 km altitude. Peak structure is also evident in the tropical cirrus layer in Figure 1c. For moderate cloud optical thickness, it is seen in these types of radiance profiles that the radiance profile returns back to the clear sky average below the radiance peak. Finally, an opaque cloud example is presented in Figure 1d, in which the radiance varies little below 15 km altitude.

[11] The altitudes in Figure 1 are AURA spacecraft toolkit values decreased by 2 km. The angular error of the HIRDLS line of sight with respect to the AURA platform is 120", as measured during on-ground spacecraft integration. Since the distance from the AURA platform to the limb path tangent point is 3012 km, an angular error of 120" corresponds to 1.7 km. By comparing HIRDLS altitude Z,

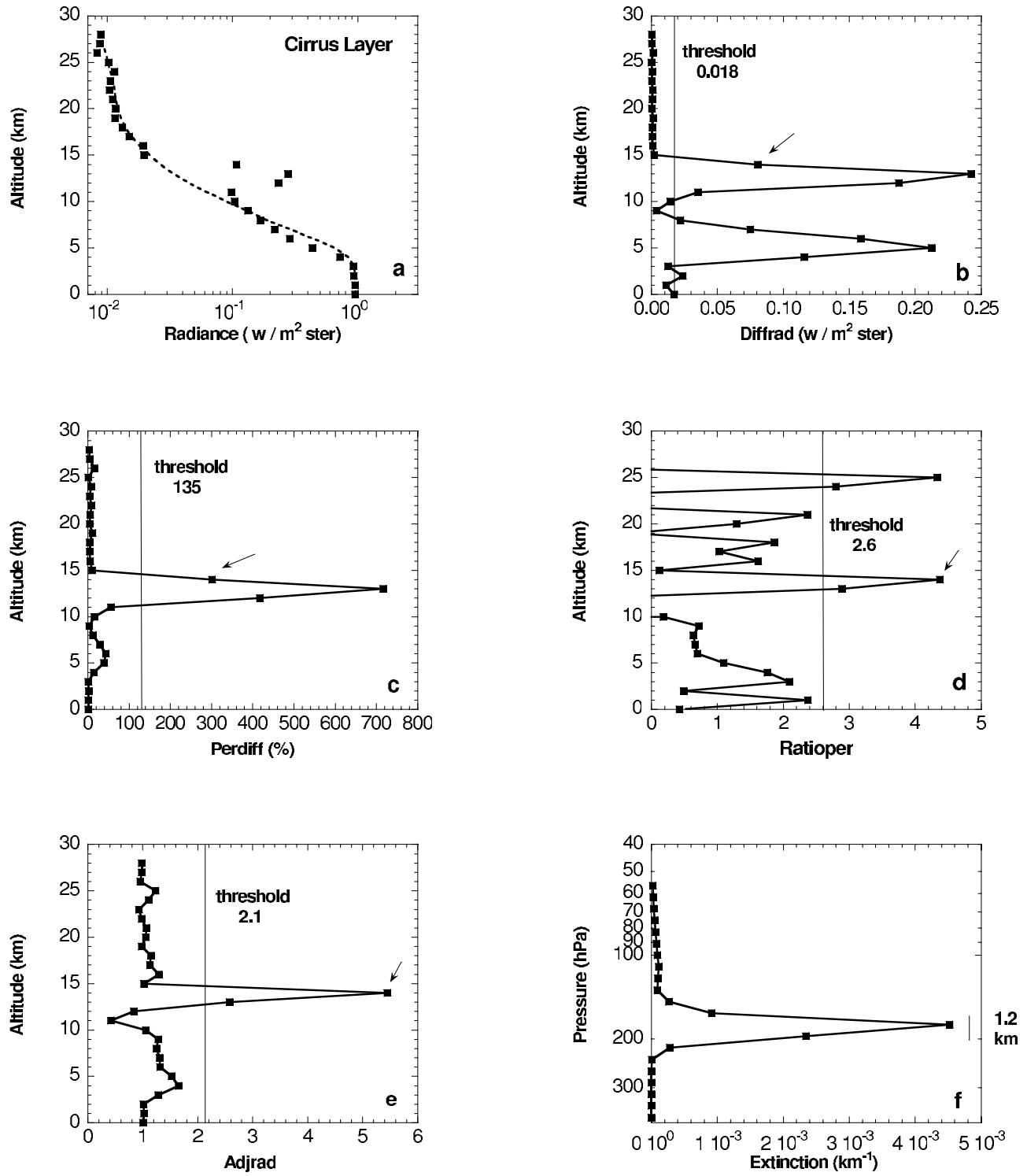

Figure 2. Illustration of the cloud detection algorithm for a single radiance profile on 18 May 2006 at 13.6°S and 314.78°E. (a) Radiance profile and the clear sky curve and (b) diffrad, (c) perdiff, (d) ratioper, and (e) adjrad curves and their respective thresholds. Arrows mark the cloud top altitude. (f) Retrieved channel 6 (12.1 μm) extinction profile. Note that the vertical width of the cirrus layer is approximately 1 km.

pressure P, and temperature T profiles to Microwave Limb Sounder (MLS) Z, P, T profiles for several days throughout the year, it was apparent that the HIRDLS profiles were higher than the MLS profiles by 2 km. This 2 km offset does not influence the retrieval of HIRDLS data, since the retrieval state vector is expressed in terms of an evenly spaced altitude grid.

[12] Using a tropical cirrus layer observation as an example, Figures 2 illustrates the specifics of the first step in the cloud detection process. Given a clear sky average

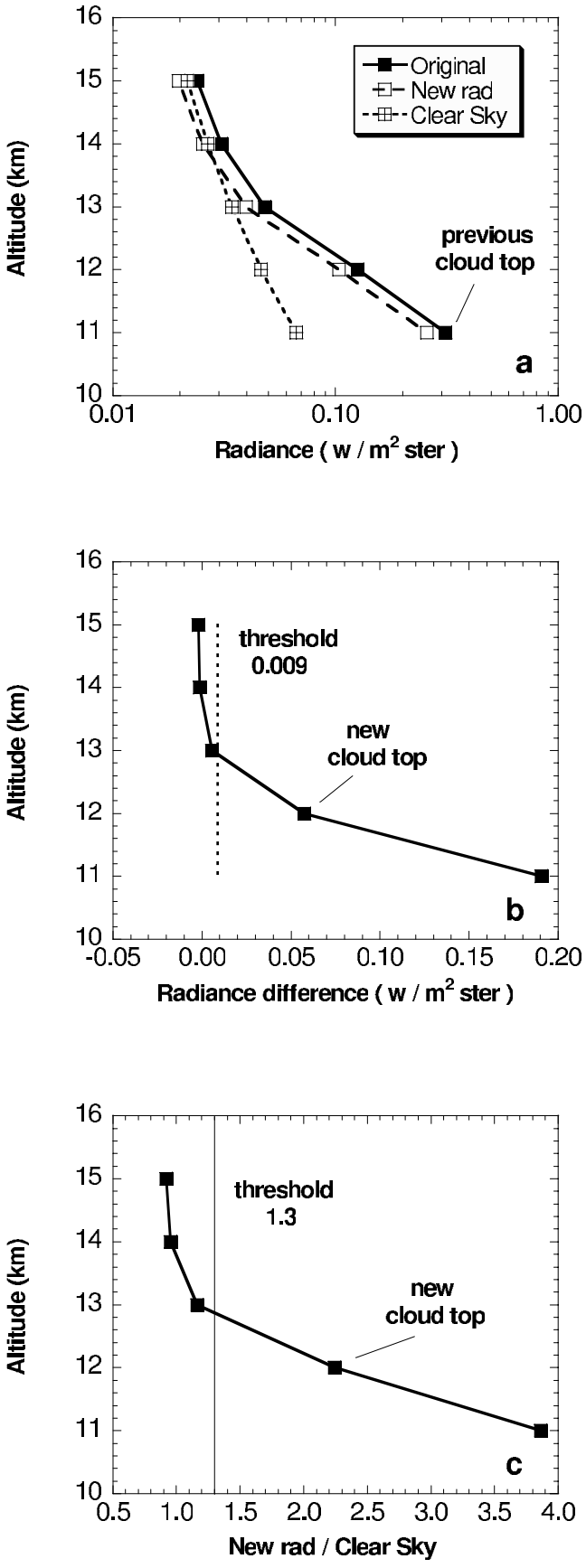

curve R_{clear} in channel 6 for a specific latitude band, cloud presence is determined in a series of tests on each individual radiance profile. Four functions are calculated, defined by the expressions

$$\text{diffrad}(i) = R_{obs}(i) - R_{clear}(i) \quad (2)$$

$$\text{perdiff}(i) = 100(R_{obs}(i) - R_{clear}(i))/R_{clear}(i) \quad (3)$$

$$\text{ratioper}(i) = (dR_{obs}(i)/dz)/(dR_{clear}(i)/dz) \quad (4)$$

$$\text{adjrad}(i) = R_{obs}(i)/R_{obs}(i+1) \quad (5)$$

[13] The four functions are calculated for an individual channel 6 radiance profile $R_{obs}(i)$ as a function of altitude index i from 1 to 30, corresponding to 1 km altitude steps between 1 and 30 km. The altitude range of 1 to 30 km is chosen because PSC sighting probabilities become less than 0.01 at altitudes greater than 28 km [*Poole and Pitts*, 1994] and it is clear from altitude versus log-radiance graphs of individual profiles that HIRDLS calibrated radiances exhibit noise above 20 km altitude.

[14] Figure 2 displays a single radiance profile and the clear sky radiance profile in Figure 2a, the four functions in Figures 2b–2e, and the numerical values of empirically determined function thresholds that are associated with each of the four functions. The first determination of the cloud top corresponds to the highest altitude level (marked by the arrows in Figure 2) for which the perdiff, ratioper, or adjrad functions exceed the thresholds, and for which diffrad is greater than the threshold of 0.018 w m^{-2} $ster^{-1}$. While ratioper exceeds the threshold value of 2.6 at 25 km altitude, diffrad is less than the diffrad threshold in Figure 2b, so the algorithm does not specify a cloud top at 25 km. The thresholds were selected by a trial and error process such that false positives in cloud detection are avoided, yet numerous graphs of altitude versus log-radiance displayed cloud tops at the altitudes determined by the algorithm. If the thresholds are decreased, then cases arise that produce false clouds (i.e., radiometric noise triggers the presence of a false cloud). At this stage of the processing, the cloud type is unknown.

[15] Since there are variations in individual temperature profiles within a given latitude band, it is expected that the clear sky radiance profile may be offset from the observed radiance profile. To account for these variations, a cloud top adjustment process is used and illustrated in Figure 3. In this particular case, the previous portions of the algorithm determined a cloud height Z_{cloud} at 11 km (see Figure 3a). The observed radiance profile is shifted along the radiance

Figure 3. Illustration of the cloud top adjustment process. Radiances are for a single profile on 18 May 2006 at 6.91°N and 221.11°E. (a) Original radiance profile, "New rad" profile, and the clear sky profile. (b) Difference in radiance of the "New rad" and clear sky profiles, and the radiance difference threshold. (c) Ratio of "New rad" to clear sky profiles and ratio threshold. For this particular case, the cloud top is shifted upward from 11 to 12 km altitude.

x axis such that the shifted radiance profile $R(i)_{new}$ lies over the clear sky curve $R(i)_{clear}$ for altitudes between 13 and 15 km (i.e., a 3 km range commencing 2 km above the Z_{cloud} cloud top altitude). The adjustment process tests if the ratio $R(i)_{new}/R(i)_{clear}$ is greater than the empirical threshold of 1.3, and if the radiance difference $R(i)_{clear} - R(i)_{new}$ is greater than the empirical value of 0.009 w m^{-2} $ster^{-1}$ at altitudes above Z_{cloud}. For this particular case, the ratio and radiance differences were sufficiently large enough to warrant a change in cloud top altitude. Figure 3c illustrates that the cloud top is moved upward from 11 to 12 km altitude.

[16] Individual tests are carried out on each radiance profile to determine the cloud type. A cirrus layer is identified if the vertical full-width half-max of the radiance perturbation is less than 4 km. Previous spaceborne lidar observations of cirrus demonstrated that thin cirrus near the tropopause can be on the order of 0.5 km thick [*Winker and Trepte*, 1998]. The small vertical widths of the HIRDLS radiance profile perturbations of "cirrus layer" clouds and the narrow width of retrieved extinction profiles (see Figure 2f), are consistent with the previous lidar measurements and ongoing measurements by the CALIPSO satellite lidar experiment. A probability distribution function (not shown) of CALIPSO cloud widths, based upon our analysis of tropical CALIPSO Clay (cloud layer) file data between 13 and 16 km altitude in August 2006, indicates that 84% and 1.5% of cirrus layers that are above clear sky regions have vertical widths less than 1.5 km and greater than 3 km, respectively.

[17] An opaque cloud in the tropics and midlatitudes is determined if the radiance profile varies slightly over a 6 km range of altitude (see Figure 1d). If the radiance profile does not adhere to the specific profile characteristics of the cirrus layer and opaque cloud, then the cloud is deemed to be of unknown type. Physically, it is expected that cloud structure will vary from that of isolated cirrus layers of small vertical width to deep convective structure throughout the tropopause. Cirrus layers are produced by the uplift of humid layers that are far away from deep convection, and by convective blow-off from deep convection. As deep convection dissipates, the cloud structure will be less opaque, and of intermediate thickness between the two extremes. These clouds are labeled by the cloud detection algorithm as of unknown type. It is also possible to have multilayer cloud structure of unrelated clouds traveling in different directions at different altitudes. These cloud structures will also be labeled as of unknown type.

[18] PSC radiative structure, similar to that presented in Figure 1b, are searched for only at latitudes greater than 50°N or less than 50°S. A straight line is fitted between the radiances of a single profile at 17 and 29 km, and the ratios of observed radiance to the straight line values are calculated between these altitudes. PSCs are flagged at altitudes at which the ratios exceed a fixed ratio threshold of 1.5 that was empirically derived in sensitivity tests. The threshold was chosen to avoid false cloud detections.

[19] The radiance signature in Figure 1b is of a PSC for which the radiance perturbation is large and "extensive" in its altitude range. The cloud detection algorithm also detects PSCs that have a lesser radiance perturbation and/or less extensive range in altitude, and labels these PSCs as of unknown type. Since the cloud detection routines are applied prior to the temperature profile retrieval, the total number of PSCs is equal to the number of extensive and unknown cloud types that are observed above the polar tropopause, which is determinable after the temperature profile is retrieved.

[20] The cloud detection routine assigns a value of 0 to all altitudes at which the radiance profile does not deviate significantly from the clear sky average. Cloud types of 1 = unknown cloud type, 2 = cirrus layer, 3 = extensive PSC, and 4 = opaque cloud are assigned according to the tests described above at each 1 km step in altitude. The integers are stored in HIRDLS "12.1MicronCloudAerosolFlag" arrays contained in archived data files available from the NASA GFSC Earth Sciences (GES) Data and Information Services Center (DISC). In addition, there is a test to determine if the radiance profile is obviously bad, e.g., that the radiance values are negative or display excessive back and forth swings in radiance. These cases usually are seen only at altitudes above 20 km.

[21] The cloud identifications above are motivated by the shapes of radiance profiles. Opaque clouds in the tropics and midlatitudes, and extensive PSCs at latitudes poleward of 50°S and 50°N, are both "opaque" in terms of the large optical depths associated with the clouds. Also, it should be noted that there is not a strict one to one correspondence between cloud locations along the vertical pressure grid at the tangent ray point and our cloud flags. Clouds can exist along the HIRDLS limb view raypath at a variety of altitudes along the raypath, and the radiance at a specified tangent height altitude is influenced by cloud optical depths at higher altitudes.

[22] While the cloud detection routines specifically label a cloud type as a PSC in the polar latitudes, radiance perturbations at nonpolar latitudes are also detected. Nonpolar volcanic and forest fire smoke clouds in the troposphere and stratosphere will be detected by the HIRDLS experiment and assigned by the cloud detection routines with the "unknown cloud" label.

[23] The cloud detection routines, in conclusion, specify the altitude at which a cloud top is determined, and assign a cloud type integer at each 1 km altitude level between 30 km and the ground. Once the retrieval of the pressure-temperature profile is completed, a cloud type integer is assigned to each of the standard pressure levels of the HIRDLS retrieval for each radiance profile, and a cloud top pressure is determined.

3. Retrieval Methodology

[24] The HIRDLS retrieval algorithm is described in detail by R. Khosravi et al. (Overview and characterization of retrieval algorithms for the High Resolution Dynamics Limb Sounder, manuscript in preparation, 2007, hereinafter referred to as Khosravi et al., manuscript in preparation, 2007). The algorithm is based on optimal estimation theory, using the maximum a posteriori solution method [*Rodgers*, 2000]. The objective of this approach is to obtain vertical profiles of atmospheric constituents for which the algorithm's radiative transfer model generates radiances that are consistent with measured radiances. The solution is constrained by prior knowledge of the atmospheric state and the measurement uncertainties.

[25] Pressure-temperature and gas mixing ratios, and cloud and aerosol extinction profiles are retrieved using two different configurations of the retrieval code. This is necessary at this point in time since the radiance calibrations of the 21 HIRDLS spectral channels are not of uniform accuracy, because of the difficulties of the Kapton obscuration, and the exact variations of the percentage of Kapton obscuration for the HIRDLS channels are being refined. The Kapton radiance field impacts the HIRDLS channels that sense the stronger CO_2 and O_3 atmospheric emissions less so (in a relative manner) than the HIRDLS channels that sense the relatively weaker emissions of the other gases.

[26] Visual examination of log-radiance versus altitude graphs for the 21 HIRDLS channels reveals that a majority (i.e., 17 out of 21) of the HIRDLS channels are perturbed by tropospheric clouds and PSCs. Retrievals of temperature-pressure and gas mixing ratio profiles assume that the channel 6 cloud top pressure applies equally well to all other channels.

[27] The operational retrieval is currently configured to retrieve the pressure-temperature (PT) profile in an iterative manner on a fixed set of pressure levels between 400 and 0.1 hPa (Khosravi et al., manuscript in preparation, 2007; Gille et al., submitted manuscript, 2007). HIRDLS channels 2–5 at 14.9, 15.5, 16.0, and 16.5 μm, which are dominated by a range of relative CO_2 opacity, are used in the PT retrieval. Climatology gas (e.g., O_3 and H_2O) mixing ratio profiles and a sulfate aerosol extinction profile (discussed below) are fixed in the PT retrieval. Input to the retrieval includes radiance profiles for the four channels, expressed at 1 km altitude steps on an evenly spaced altitude grid. The 2 km offset mentioned in the previous section does not influence the retrieval, since the retrieval state vector is expressed in terms of an evenly spaced altitude grid. Retrieved profile-specific PT values are interpolated to the standard AURA pressure grid of the archived data files.

[28] If a cloud is detected by the cloud detection routines, then the iterative matrix solution increasingly weights the retrieval below the cloud top by a priori values. Negative temperature and gas mixing ratio precisions flag cases in which the a priori error contributes more than 50% to the total error, indicating large a priori contributions to the retrieval. It is recommended that users not use temperature values, gas mixing ratios, and cloud/aerosol extinction values that are assigned negative precisions.

[29] HIRDLS channels were specifically selected to focus upon the retrieval of gas species (i.e., O_3, HNO_3, H_2O, NO_2, N_2O, CH_4, CFC-11, CFC-12, $ClONO_2$, and N_2O_5). *Edwards et al.* [1995] describes the selection of the HIRDLS gas radiance channels. The retrieved pressure-temperature profile, climatology gas mixing ratios, and a single aerosol sulfate extinction profile (discussed below) are fixed in the gas retrievals. The retrieved mixing ratios are interpolated from the profile-specific pressure grid to the standard pressure grid of the archived data files. Negative gas mixing ratio precisions flag cases in which the a priori error contributes more than 50% to the total error.

[30] The retrieval of cloud and aerosol extinction requires knowledge of the temperature-pressure profile and the mixing ratios of gas species. The relative contributions of gas and background sulfate aerosol to the HIRDLS limb radiances at 25 km altitude can be viewed by examination of the 0.5 cm^{-1} resolution spectra of *Edwards et al.* [1995]. Line-by-line spectral calculations were used to determine the wavelength ranges of the HIRDLS channel filters. Five channels, centered at 17.4, 12.1, 10.8, 8.3, and 7.1 μm (channels 1, 6, 9, 13, and 19, respectively) were specifically chosen because the ratio of aerosol/cloud optical depth to gas optical depth is relatively high at these wavelengths. In particular, the 12.1 μm window channel (channel 6) is widely known to have the lowest gas optical depths in the infrared, and is the most sensitive HIRDLS channel for the detection of cloud extinction. CO_2 spectral lines dominant the gas opacities in the 12.1 μm channel.

[31] The current operational processing solves for aerosol/cloud extinction and temperature profiles by configuring the retrieval code in the following manner, which is run separately from the retrieval of temperature profiles and gas mixing ratios that is described above. The retrieval ignores the cloud top height, and retrieves the temperature profile throughout the full range. This temperature profile is then used to retrieve cloud/aerosol extinctions throughout the full altitude range. Extinction profiles are independently retrieved for channels 1, 6, 9, 13, and 19. Gas species (e.g., O_3, HNO_3, and H_2O) are specified based upon the latitude and time-of-year-dependent MOZART (Modeling of Ozone and Related chemical Tracers) climatology, since inclusion of retrieved gas mixing profiles directly into the cloud/aerosol extinction retrievals awaits further improvements in the accuracy of the HIRDLS radiance profiles. MOZART is a 3-D chemical transport model [*Kinnison et al.*, 2007] that is used for the a priori gas mixing ratio fields and the initial guess in the HIRDLS retrieval. A single midlatitude SAGE (Stratospheric Aerosol and Gas Experiment) aerosol extinction profile is used to specify the cloud/aerosol a priori. A Mie calculation was used to transform the SAGE extinction at 0.525 μm to the wavelengths of the five HIRDLS cloud/aerosol channels. If the retrieval has difficulty converging, then the retrieval assigns an extinction value equal to -999 at all pressure levels.

[32] Precisions are reported along with the extinction values for the five HIRDLS cloud/aerosol channels. The precision at a retrieved pressure level is the measured extinction times the square root of the diagonal element of the solution error covariance matrix. The covariance matrix is evaluated during the retrieval iterations by the Optimal Estimation algorithm [*Rodgers*, 2000], and incorporates radiometric channel noise, smoothing error, forward model error, and forward model parameter error [*Lambert et al.*, 1999]. Negative precisions flag cases in which the a priori error contributes more than 50% to the total error.

[33] Stratospheric sulfate aerosol extinctions are preliminary since the gas and sulfate aerosol opacities are of similar magnitude, and the current retrieval uses climatology gas opacities. Aerosol retrieval accuracy will improve when the radiances of the HIRDLS experiment become more precise and coupled retrievals of pressure-temperature, O_3, H_2O, and channel 6 extinction become appropriate.

4. Measurements of Cloud Top Pressure

[34] Cloud top pressures are determined once the pressure-temperature profile is retrieved. The altitude integer index is determined by the cloud detection algorithm

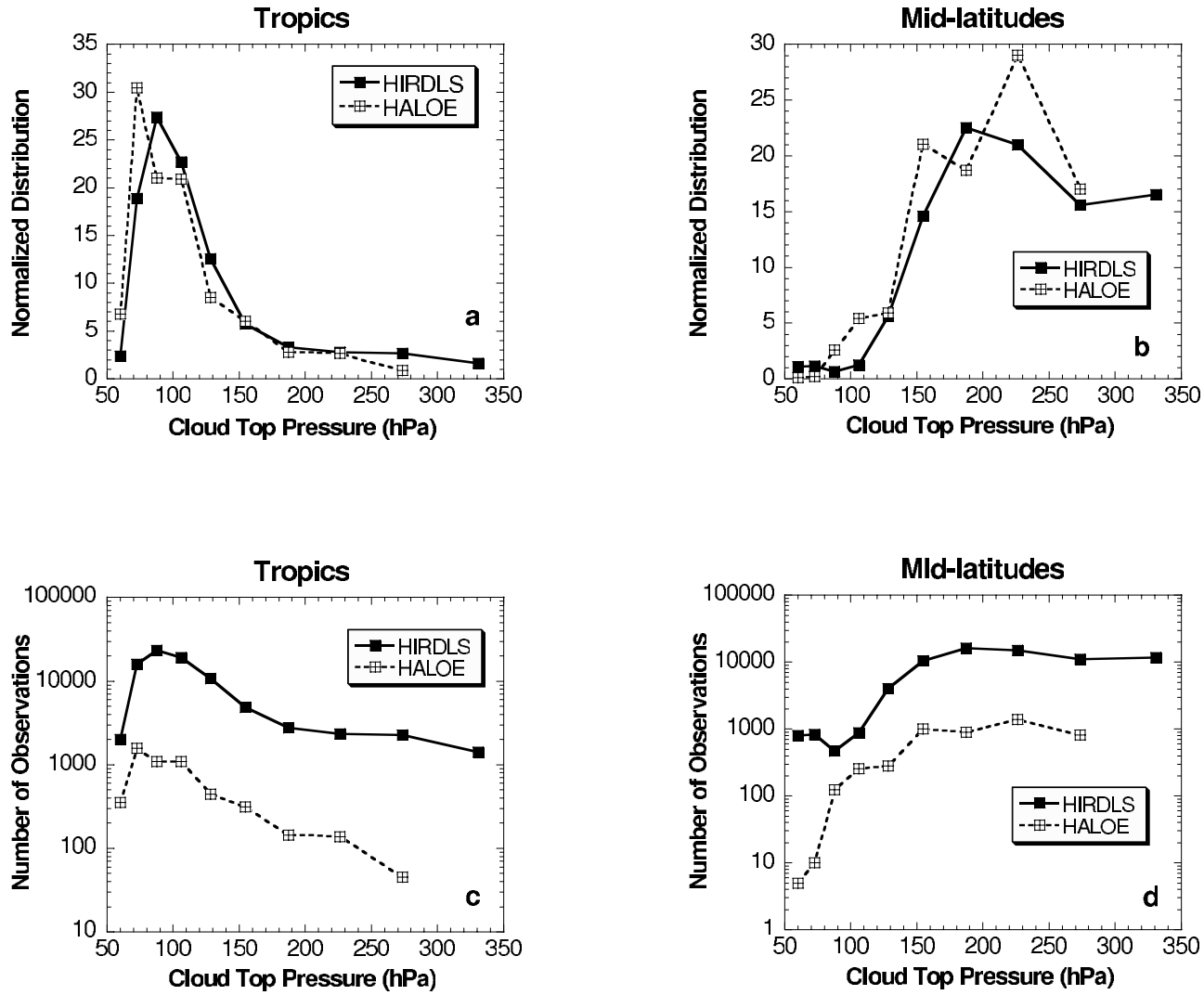

Figure 4. (a and b) Comparison of the normalized distributions of HIRDLS and HALOE cloud top heights for the tropics (20°S–20°N) and midlatitudes (55–35°S, 35–55°N). HIRDLS observations are from 2005, while the HALOE observations are from 1998 to 2005. (c and d) Number of observations for the pressure ranges.

described in section 2, and the pressure of the cloud top is the pressure associated with the profile-specific pressure-temperature retrieval (i.e., the cloud top pressure is not interpolated unto the standard HIRDLS archived pressure grid). We compare HIRDLS cloud top pressures to those derived from version 19 HALOE and SAGE III data files in this section of the paper.

[35] HALOE [*Russell et al.*, 1993] made measurements from the Upper Atmosphere Research Satellite (UARS) from September 1991 through November 2005. Validation of the aerosol extinction data at 3.46, 3.40, 2.45 and 5.25 μm is discussed by *Hervig et al.* [1996]. SAGE III made solar occultation measurements between 45°N and 80°N, and 35°S and 60°S between March 2002 and December 2005. Extinction measurements [*Thomason et al.*, 2007] are reported at 385, 449, 521, 600, 676, 755, 868, 1020, and 1545 nm. The multiwavelength technique used to determine cloud top pressures is discussed by *Kent et al.* [2007]. The ratios of 525 nm to 1020 nm and 1020 nm to 1550 nm extinction are expected to approach unity as particle size becomes large. If observed values of these two ratios, graphed on a ratio-ratio graph, fall within a specific trapezoid that overlies the unity ratio value [see *Kent et al.*, 2007, Figure 5], then a cloud is identified by the SAGE III algorithm.

[36] Cloud top pressures are not reported in the archived HALOE data files. We determine the presence of clouds for each HALOE observation by examining the numerical value of the spectral variance (ψ^2) of the HALOE extinction spectrum [*Hervig and McHugh*, 1999]. Values of ψ less than 0.1 approximately correspond to the presence of clouds. HALOE 3.46 μm extinction greater than 4.0×10^{-4} km^{-1} consistently have ψ values less than 0.1 [*Massie et al.*, 2002]. The physical basis for this relationship is due to the fact that the wavelength dependence of extinction spectra flatten out as particle size increases. Sulfate particles have radii on the order of 0.1 μm, and ψ values greater than 0.1. Cirrus radii are larger than $\sim$5 μm, and result in

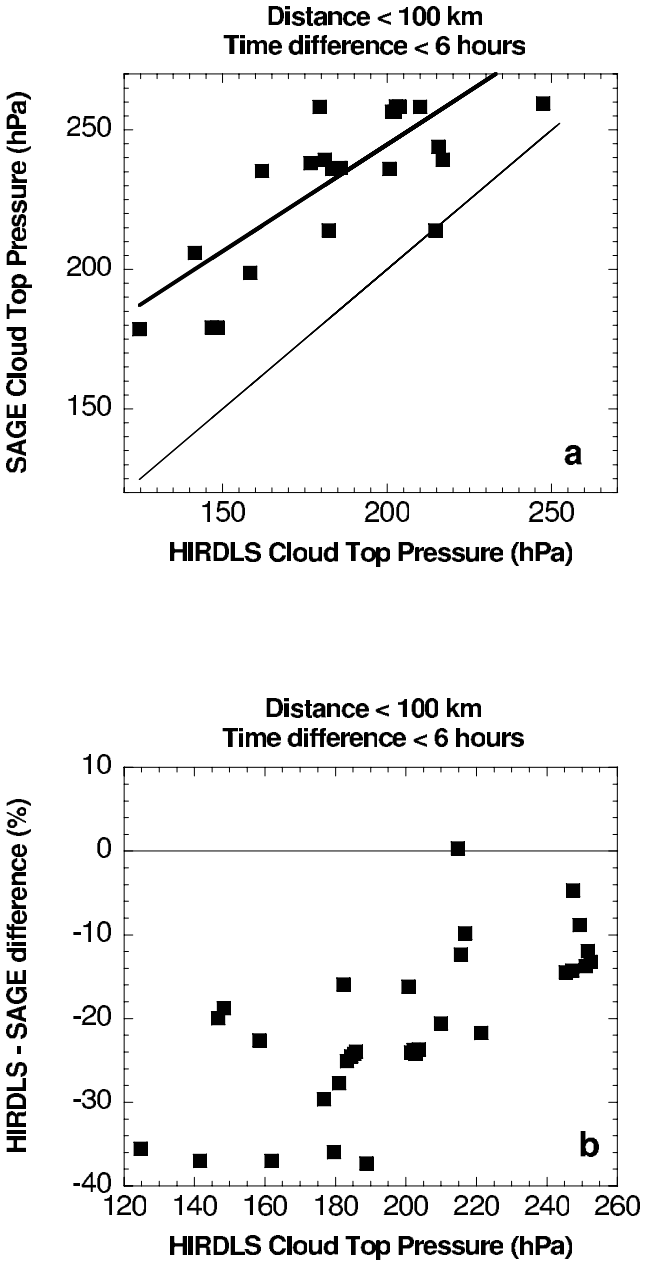

Figure 5. (a) SAGE and HIRDLS cloud top pressure comparisons in 2005 for southern midlatitudes and latitudes north of 70°N. The two sets of cloud top pressures have a correlation coefficient of 0.85 when the distance between observations is less than 100 km and the time difference is less than 6 h. (b) Percent differences in the HIRDLS and SAGE cloud top pressures.

extinction spectra that are much flatter than the extinction spectra of sulfate particles.

[37] Using this multiwavelength technique, HALOE extinction data from 1998 to 2005 were processed to calculate HALOE cloud top pressures. HALOE data from 1998 to 2005 were analyzed since there are few (~55) HALOE cloud observations in 2005. Values of ψ were calculated at all of the HALOE pressure levels for each HALOE extinction profile. Working down from the top altitude of the profile, the cloud top pressure was determined when ψ became less than 0.1. HALOE cloud top pressures were binned into two sets of latitude ranges, i.e., the tropics (20°S–20°N) and midlatitudes (55–35°S, 35–55°N). For each of the binned sets of HALOE cloud top pressures (see Figures 4c and 4d), normalized distribution curves in Figures 4a and 4b were calculated for nine log-pressure bins between 40 and 400 hPa by normalizing each of the curves in Figures 4c and 4d to unity. HIRDLS cloud top pressures were binned in the same manner.

[38] Figures 4a and 4b compare the normalized HIRDLS and HALOE distributions. The normalized distributions are very similar for the two latitude ranges, both in the shapes of the curves and in the range of pressure over which the shapes are similar. Differences in the number of observations are due to the fact that HIRDLS makes a measurement every 10 s, while the HALOE occultation experiment measured 32 profiles per day. The correlation coefficients of the normalized distributions of the cloud top pressures in Figures 4a and 4b for the tropics and midlatitudes are 0.87 and 0.93, respectively.

[39] It is apparent that the HALOE cloud top pressure averages are at slightly lower pressures than those of HIRDLS. A difference in 1 km in Figure 4 at pressures near 100 hPa, which is the granularity of the HIRDLS radiance profile grid, corresponds to a pressure difference between 85 and 100 hPa, and is on the order of the difference in pressure of the HALOE and HIRDLS cloud top curves in Figure 4 at 70 hPa in the tropics and 150 hPa in the midlatitudes. The reason for these differences are not known at present, but may be due to the sensitive capability of the multiwavelength HALOE technique, relative to the HIRDLS technique, to detect very tenuous clouds. The HIRDLS single wavelength technique is constrained by several threshold limits (see Figures 2 and 3). The HALOE technique looks at the spectral variance of multiwavelength extinction, which is not dependent upon the magnitude of the extinction.

[40] Comparisons of HIRDLS and SAGE III cloud top pressures in 2005 are presented in Figure 5. Because of the geographical sampling characteristics of the SAGE III and HIRDLS experiments, the comparisons are derived from data at southern midlatitudes and latitudes north of 70°N. Figure 5a presents a scatterplot of HIRDLS and SAGE III cloud top pressures when the distance between the observations was less than 100 km, and the time difference was less than 6 h. The correlation of the data points is 0.85. The light solid line is the 1 to 1 line, while the solid line is the fit to the two data sets. There is a systematic offset between the two data sets, with HIRDLS data points being at lower pressures by ~20% (see Figure 5b). A 20% pressure difference corresponds to a vertical distance of 1.3 km for a representative scale height of 7 km.

[41] Table 1 presents the correlation coefficients of the SAGE III and HIRDLS cloud top pressures expressed as a function of separation in distance and time, from 0–100, 0–200, 0–300, 0–400 km, and for time separations of 0–6, 0–12, 0–18, and 0–24 h. The number of data points for the samplings varied from 531 for the 0–400 km and 0–24 h comparison, to 32 for the 0–100 km and 0–6 h comparison. The correlations vary between 0.45 and 0.85, depending upon the time and space difference. Table 1's values indicate that the correlation improves significantly if the

Table 1. Sensitivity of HIRDLS and SAGE III Cloud Top Pressure Correlations to Observation Distance and Time Separations

	Time, hours			
Distance, km	0–6	0–12	0–18	0–24
0–100	0.85	0.85	0.59	0.55
100–200	0.77	0.75	0.57	0.54
200–300	0.72	0.68	0.51	0.49
300–400	0.64	0.62	0.45	0.45

time and space differences decrease. This is expected, since clouds are very transitory. The data in Table 1 indicate that low correlation coefficients between two cloud data sets may be due primarily to the transitory nature of cloud structures, and not necessarily due to instrument deficiencies.

5. Observations of Polar Stratospheric Clouds

[42] In this section we comment on the PSC counting statistics of the HIRDLS experiment, demonstrate that the counting statistics are physically realistic, and present preliminary PSC and sulfate extinction for a single day's observations.

[43] Figure 6a displays time series of the number of PSCs observed by HIRDLS each day in January and February 2005 for potential temperatures between 440 and 460 K. HIRDLS began observations on 23 January 2005 (the time of the first data point in Figure 6a), and did not observe PSCs in March of 2005. Three curves are presented in Figure 6a. The lowermost curve is the number of PSCs identified by the cloud detection algorithm to be similar to the radiance signature of Figure 1b (i.e., the "extensive" PSCs). The middle curve presents the number of "unknown" clouds that were flagged by the cloud detection routine, and which were located at positions northward of 55°N, for which post PT retrieval HIRDLS temperature values were less than 200 K and potential temperatures were between 440 and 460 K. HIRDLS temperatures in the presence of clouds, when compared to Microwave Limb Sounder (MLS) temperatures, have a 2–4 K warm bias (since cloud/aerosol opacity is not solved for in the PT retrieval). In the absence of clouds, the HIRDLS and MLS temperatures agree very well (Gille et al., submitted manuscript, 2007). The 200 K threshold was selected to allow for this warm temperature bias in order to approximate a temperature threshold of 195 K, the temperature threshold for which microphysical models initiate nitric acid trihydrate (NAT) formation [*World Meteorological Organization*, 1999]. The total number of PSCs observed per day is given by the sum of the unknown and extensive PSC curves. Over100 PSC profiles per day were observed by the HIRDLS experiment from late January through mid-February.

[44] Figure 6b presents the time series of the hemispherical fraction (in percent) of the polar region which had temperatures less than 195 K on the 450 K potential temperature surface. The number of observed PSCs per day increases as the fractional area increases in Figures 6a and 6b. In late March both the PSC counts and fractional area decreases substantially as cold polar temperatures disappear. The correlation coefficient of the "All PSCs" and fractional area data points (not shown) is 0.92 for a sample size of 27 points.

[45] Because of the viewing geometry of HIRDLS that is imposed upon the experiment by the Kapton obstruction, observation latitudes range from 67°S to 80°N. If there were no blockage, then the observation latitude range would be from 90°S to 90°N. PSCs are detected in the southern polar

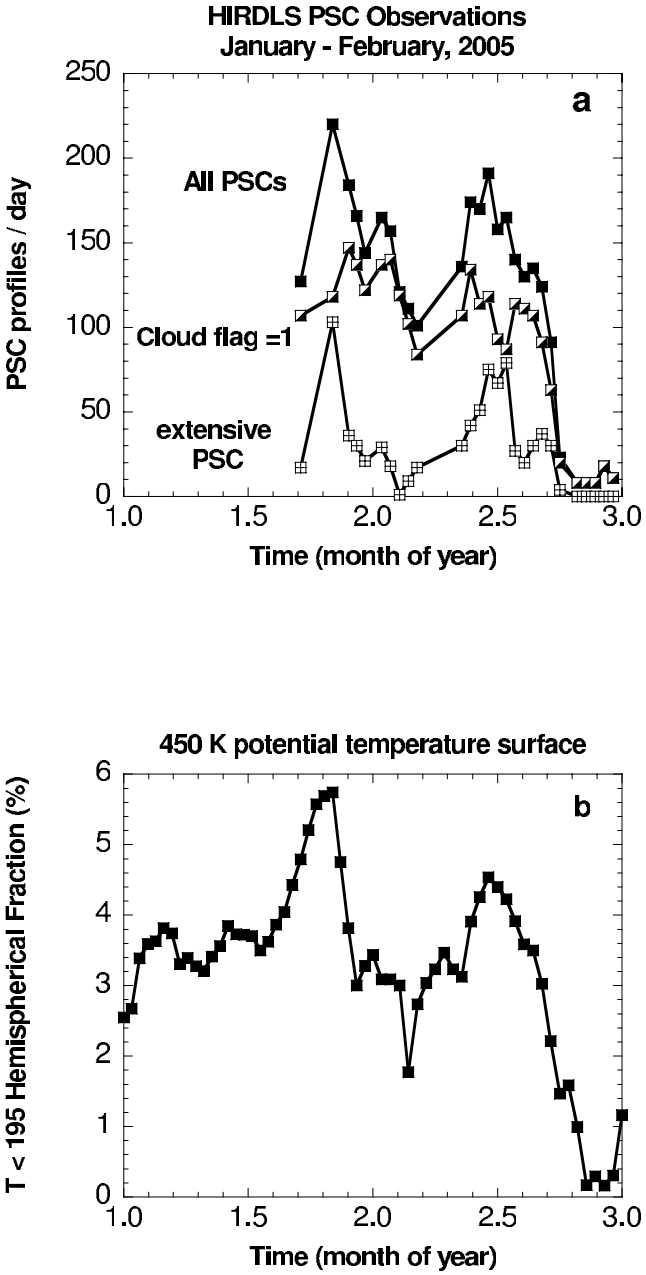

Figure 6. (a) Number of PSCs observed per day in the 440–460 K potential temperature range when the HIRDLS retrieved temperature is less than 200 K. The "extensive PSC" and unknown cloud ("cloud flag = 1") curves are added to obtain the "All PSCs" curve. HIRDLS observations started on 23 January 2005 (fractional month time of 1.7). (b) Hemispherical fraction on the 450 K potential temperature surface, for which temperatures are less than 195 K, derived from GEOS-4 data.

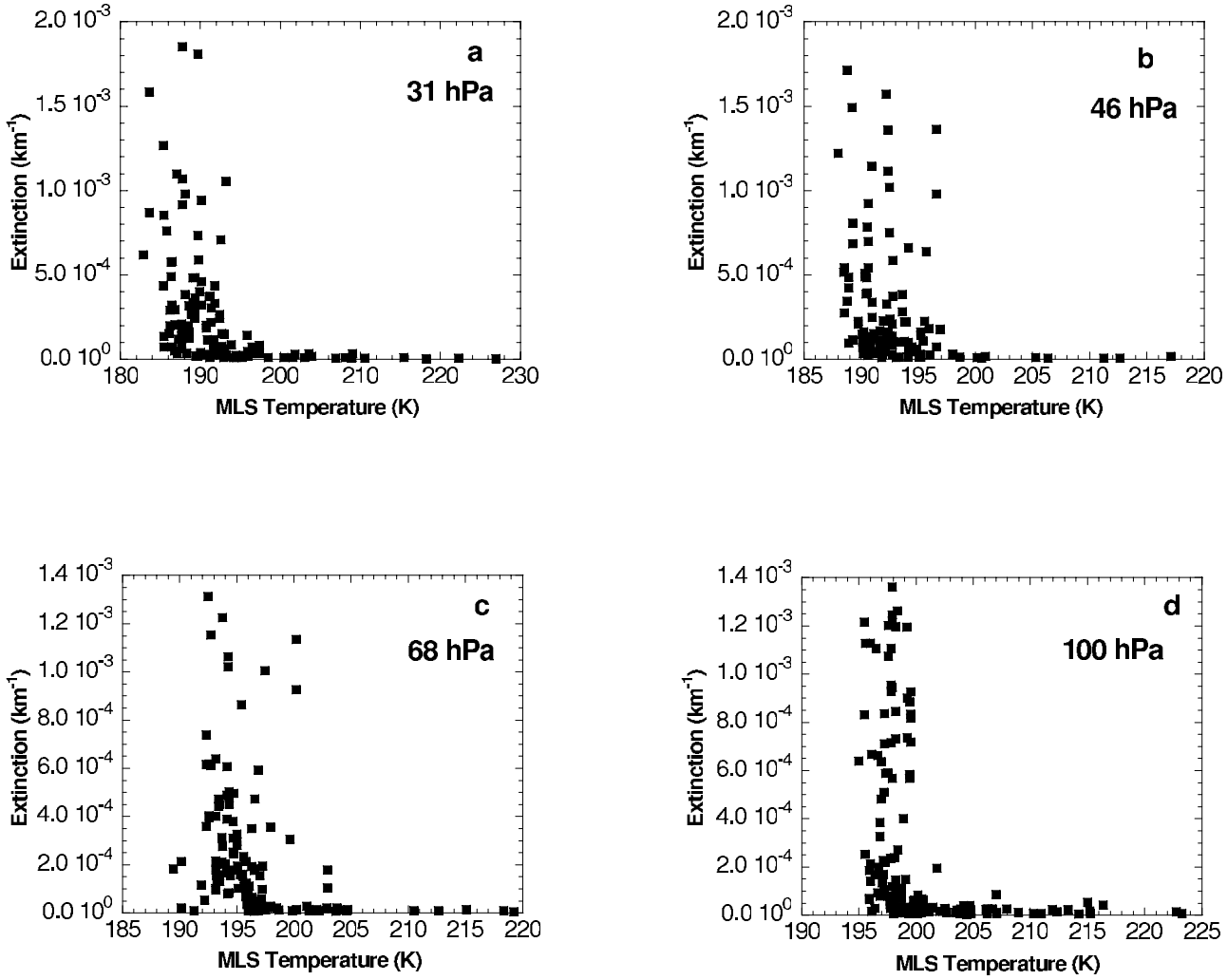

Figure 7. HIRDLS 12 μm extinction versus MLS temperature at (a) 31, (b) 46, (c) 68, and (d) 100 hPa on 27 January 2005 at latitudes between 55 and 90°N. Distances between the HIRDLS and MLS observations are less than 150 km.

vortex only when the polar vortex extends northward of 67°S. HIRDLS did observe, however, an average of 65 and 48 PSC profiles per day in July of 2006 and 2005, respectively.

[46] Figure 7 presents scatterplots of HIRDLS 12.1 μm extinction versus MLS temperature on a single day, 27 January 2005, at 31, 46, 68, and 100 hPa. Distances between the HIRDLS and MLS observation points are less than 150 km. MLS temperatures were used to prepare the graphs because of the 2–4 K warm bias in the HIRDLS data as temperatures decrease below 200 K when clouds are present. As temperatures decrease below 195 K, NAT particles and ternary solution droplets [*Tabazadeh et al.*, 1994; *Carslaw et al.*, 1995] form, particle size, area and volume densities, and PSC extinctions increase. Examples of observations of increases in extinction as temperatures decrease are illustrated in CLAES extinction [*Massie et al.*, 1994], Improved Limb Atmospheric Spectrometer (ILAS) [*Saitoh et al.*, 2002], and POAM III [*Benson et al.*, 2006] data. Figures 7a–7d display significant increases in extinction below 195 K. All of the data points correspond to HIRDLS cloud extinction precisions better than 50%. Visual inspection of the graphs suggest that HIRDLS 12.1 μm extinctions above 2×10^{-4} km^{-1} at temperatures below 195 K for pressures between 31 and 100 hPa are reliable indicators of the presence of PSCs.

[47] We attempted to match HIRDLS extinction measurements with Polar Ozone and Aerosol Measurement (POAM III), HALOE, and SAGE III extinction measurements in 2005, but found too few spatial and time coincidences. This difficulty in obtaining sufficient matches in extinction observations from different satellites was encountered, and discussed, by *Thomason et al.* [2007], who validated SAGE III aerosol extinction by using time, longitude, altitude, and Ertel potential vorticity to increase coincidences. *Thomason et al.* [2007] choose to eliminate most PSCs from their data comparisons since PSCs are spatially inhomogeneous.

6. Clouds in the UT/LS

[48] In this section we discuss the tropical cloud counting characteristics of the HIRDLS experiment, compare HIRDLS and correlative data cloud product averages, and discuss preliminary cirrus extinction values.

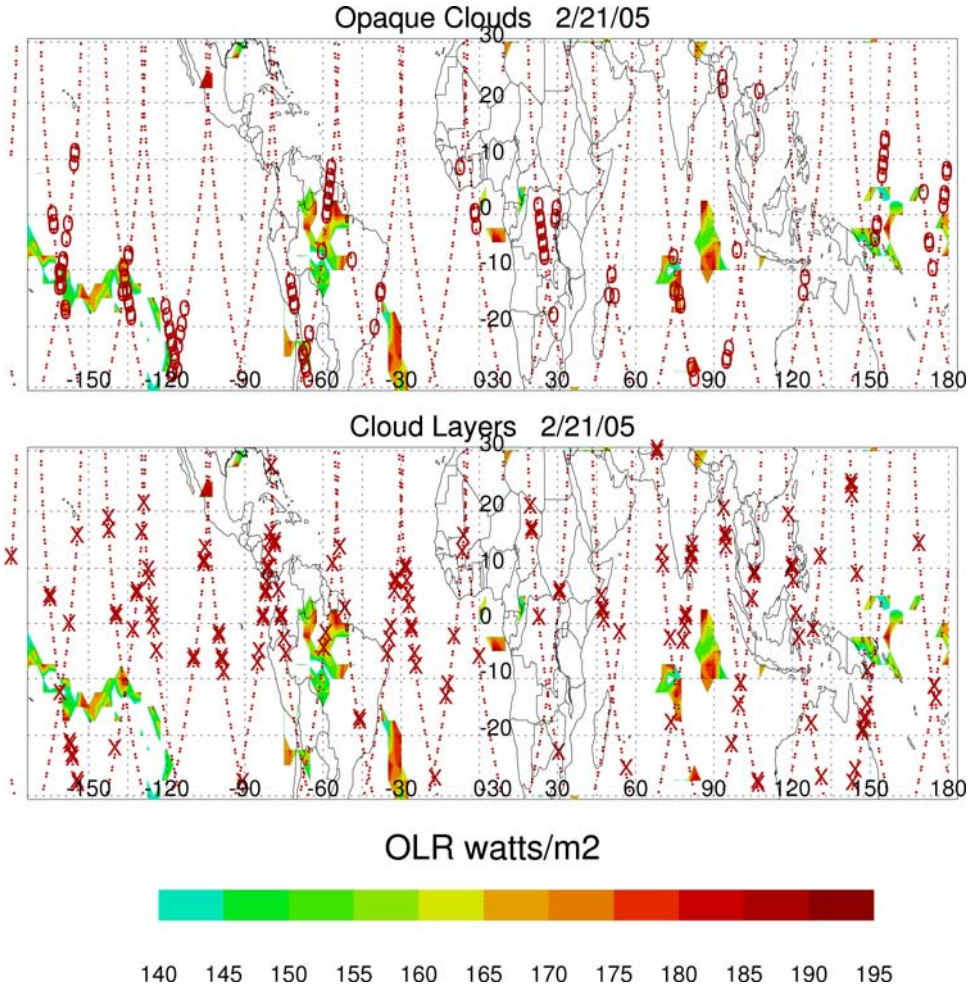

Figure 8. Locations of HIRDLS opaque clouds (circles) and cirrus layers (crosses) and tangent tracks on 21 February 2005. Opaque clouds that are associated with Climate Diagnostics Center OLR less than 190 w m^{-2} are associated with deep convection. In contrast, cirrus layers are associated with a wider range of OLR that may or may not be associated with deep convection.

[49] Figure 8 presents the locations of tropical opaque clouds and cirrus layers on 21 February 2005, the location of low values of outgoing longwave radiation (OLR), and HIRDLS tangent point tracks. High cloud tops have very low temperatures and thus emit less longwave radiation than less cloudy regions. Climate Diagnostic Center (CDC) interpolated daily mean OLR data (http://www.cdc.noaa.gov/cdc/data.interp_OLR.html) is highlighted in Figure 8 when OLR is less than 190 w m^{-2}, an approximate threshold for deep convection. If an opaque cloud is associated with OLR less than 190 w m^{-2}, then a cloud is associated with deep convection. This is especially evident in the region bounded by latitude from 30°S to the equator and by longitude from −180° to −120°W. Other opaque clouds are not associated with deep convection, with the clouds over Africa being a good example. Cirrus layers are scattered throughout the tropics. As noted by *Pfister et al.* [2001] and *Massie et al.* [2002], cirrus layers are associated with deep convection approximately half of the time. Cirrus originates from the blow-off from deep convection, and is also formed in an independent manner by the uplift of humid layers [*Jensen et al.*, 2001]. Parcel trajectory calculations reveal that subvisible cirrus is not associated with deep convection ~50% of the time over a five day timescale [*Massie et al.*, 2002].

[50] Figure 9a displays the number of cirrus layers, unknown, and opaque clouds observed in eight days in May 2006 in the tropics, as a function of colocated CDC OLR data. Most of the clouds in Figure 9a are of the unknown cloud type. Figure 9b displays the curves of Figure 9a, normalized to unity. Cirrus layers are associated, in a relative sense, more with higher OLR values (i.e., clearer sky conditions) than the opaque and unknown clouds. Figure 9c presents normalized distributions of HIRDLS and HALOE cloud observations versus OLR. The HIRDLS curve is derived from the sum of the curves in Figure 9a, and the HALOE curve is derived from the 100 hPa panel of *Massie et al.* [2002, Figure 5]. Distributions are set to unity at 270 w m^{-2}. The HIRDLS and HALOE distribution curves are very similar, and emphasize the similar statistics of cloud counting of the two experiments. The correlation coefficient of the two curves in Figure 9c is 0.99 with a sample size of 15.

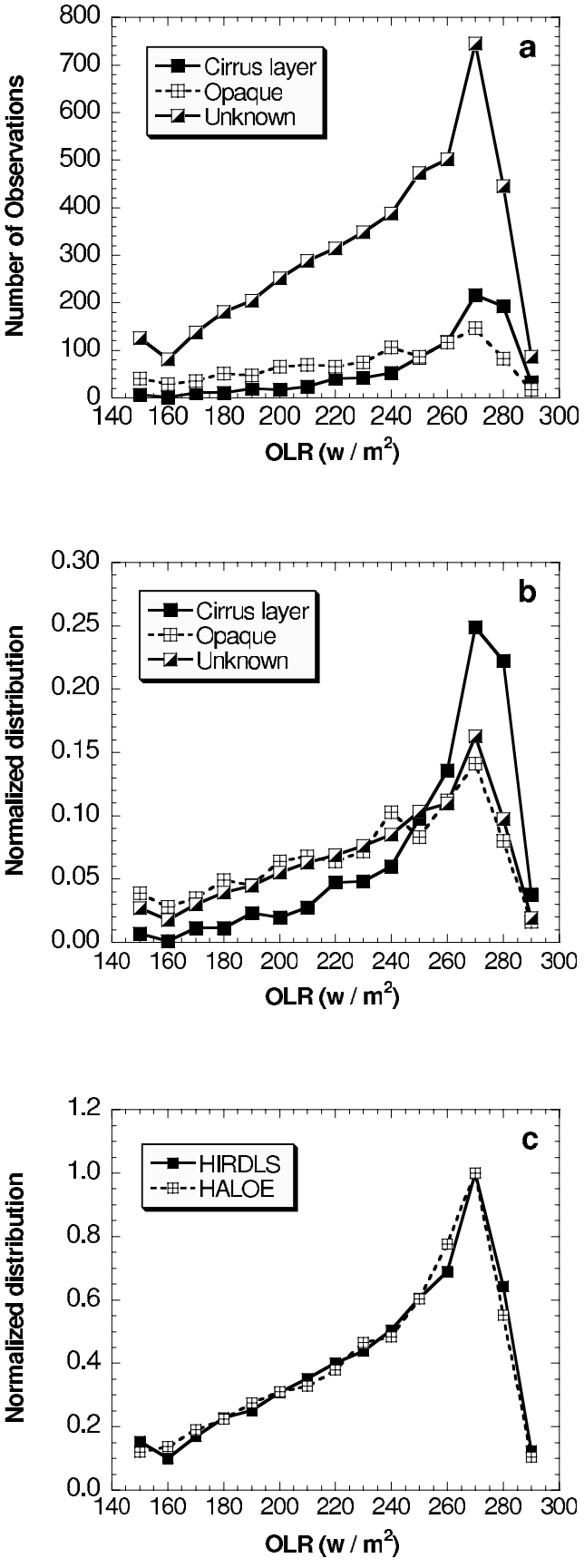

[51] Another cloud counting capability of the HIRDLS experiment is demonstrated by calculating and comparing the normalized distributions of laminar cirrus horizontal scales as measured by the CALIPSO and HIRDLS experiments. CALIPSO Clay files contain the number of cloud layers and their altitudes along CALIPSO's nadir viewing orbital track, while the HIRDLS data files contain cloud flags as a function of altitude for each radiance profile. HIRDLS cirrus layer data for 220 days during 2005–2007, latitudes between 30°S and 30°N, and altitudes between 12 and 16 km were analyzed. CALIPSO Clay data for August 2006 was analyzed for a similar latitude and altitude range, with the proviso that the difference between cloud top and cloud bottom is less than 3 km. The numbers of contiguous horizontal cloud layers were counted for horizontal bins of 0–100, 100–200, 200–300, 300–400, and 400–500 km. Though the CALIPSO experiment has a finer horizontal resolution than 100 km, the 100 km size bin was selected to match the 100.2 km spacing between consecutive HIRDLS measurements near the equator. Normalized distributions were calculated from both data sets and are presented in Figure 10. The normalized distributions are very similar, with a correlation of 0.99 and sample size of five.

[52] HIRDLS and HALOE cloud occurrence frequencies at 82 and 100 hPa are compared in Figures 11 and 12. HALOE data from 1998 to 2005 were analyzed since there are few (~55) HALOE cloud observations in 2005. As discussed above in section 4, a cloud is deemed to be observed by the HALOE experiment if the extinction spectrum ψ value was less than 0.1. HIRDLS "12.1MicronCloudAerosolFlag" array data were used to indicate the presence of clouds. Figures 11 and 12 present cloud occurrence frequencies for cases when (1) unknown and cirrus layers (cloud flags 1 and 2) and (2) unknown, cirrus layers, and opaque clouds (cloud flags 1, 2, and 4) are present. Both experiments place maximum frequency of occurrence over the maritime continent, Africa, and South America. These patterns are similar to SAGE II distributions of cloud frequency [*Wang et al.*, 1996]. The HIRDLS distributions near longitudes 130°W and 50°E are a little wider than the HALOE distributions. The cloud frequencies are larger for the HIRDLS observations in which opaque clouds are included in the calculation, as expected. The HIRDLS frequencies are calculated using radiance perturbations, while the HALOE frequencies are based upon extinctions. HALOE does not retrieve extinction if the transmission became less than 0.03, and this condition applies to some of the opaque clouds in the tropics. Table 2 presents comparisons of the cloud occurrence frequencies, averaged over the latitude range from 20°S to 20°N. The ratios of the averaged cloud frequencies are within 30% of

Figure 9. (a) Number of cirrus layers, opaque clouds, and unknown cloud types, observed by HIRDLS in eight days in May 2006 between 30°S and 30°N in the upper troposphere. (b) Curves from Figure 9a, normalized to unity. (c) Normalized distributions, set to unity at 270 w m^{-2}, of HIRDLS and HALOE cloud observations versus OLR. The HIRDLS curve is derived from the sum of the curves in Figure 9a. The HALOE curve is from *Massie et al.* [2002, Figure 5] for data from 1995 to 2000 and at 100 hPa.

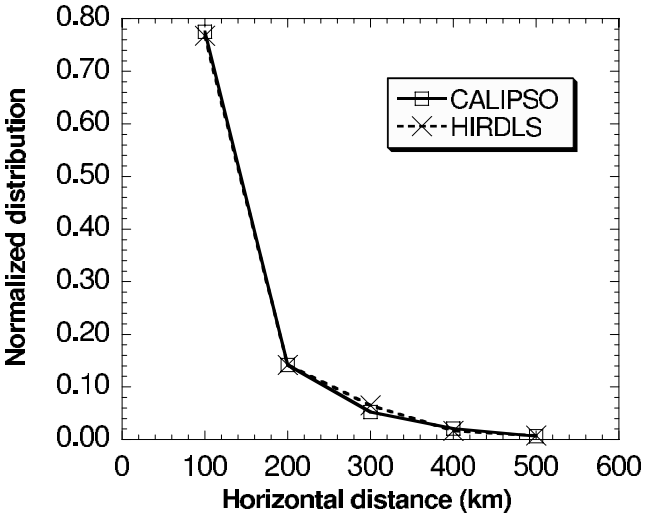

Figure 10. Normalized distributions of the contiguous horizontal lengths of laminar cirrus, determined from CALIPSO data in August 2005 and HIRDLS data from 240 days during 2005–2007, for altitudes between 12 and 16 km, and latitudes between 30°S and 30°N.

each other at 82 and 100 hPa when the HIRDLS unknown and cirrus layer clouds are used to form the ratio.

[53] Additional graphs (not shown) were prepared for the same spatial and temporal averaging as that of Figures 11 and 12 that compares HALOE and HIRDLS extinctions. Cloud extinctions between 1.0×10^{-5} and 1.0×10^{-2} km^{-1} for both experiments were used to calculate the extinction fields. The 1.0×10^{-2} km^{-1} upper limit was picked to avoid optical depths that are too large. While the HALOE 3.46 μm and HIRDLS 12.1 μm wavelengths differ, these observation wavelengths should have approximately equivalent extinction values, since Mie calculations indicate that the extinction values at 3.46 and 12.1 μm differ by less than 13% for ice cloud radii larger than 5 μm. HALOE extinctions were used in the calculations if the extinction spectrum ψ values were less than 0.1, and HIRDLS extinctions were used if the HIRDLS "12.1MicronCloudAerosolFlag" values were nonzero. Table 3 presents average extinction

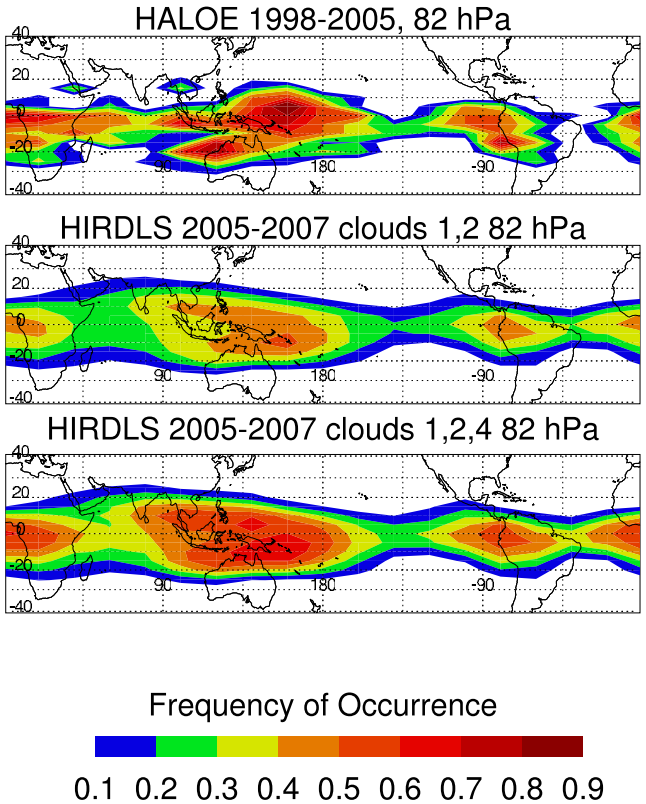

Figure 11. (top) HALOE cloud frequencies at 82 hPa from 1998 to 2005. (middle) HIRDLS cloud frequencies at 82 hPa of cirrus layers and unknown cloud types. (bottom) HIRDLS cloud frequencies for cirrus layers, unknown clouds, and opaque clouds.

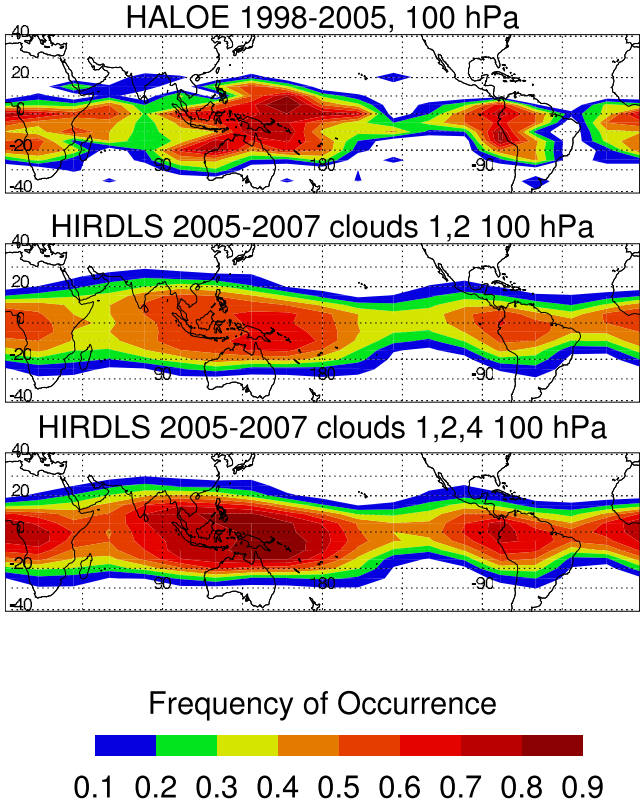

Figure 12. (top) HALOE cloud frequencies at 100 hPa from 1998 to 2005. (middle) HIRDLS cloud frequencies at 100 hPa of cirrus layers and unknown cloud types. (bottom) HIRDLS cloud frequencies for cirrus layers, unknown clouds, and opaque clouds.

Table 2. HALOE and HIRDLS Tropical Cloud Frequency Averages for 20°S to 20°N[a]

		HIRDLS		
Pressure, hPa	HALOE	Type = 1, 2	Type = 1, 2, 4	Ratio
82	0.24	0.23	0.31	0.99
100	0.30	0.37	0.48	1.21
121	0.30	0.45	0.59	1.50

[a]Cloud types 1, 2, and 4 are unknown cloud types, laminar cirrus, and opaque clouds. Ratios are calculated by dividing the HIRDLS type 1 and 2 averages by the HALOE averages.

Table 3. HALOE and HIRDLS Tropical Cloud Extinction Averages for 20°S to 20°N[a]

		HIRDLS		
Pressure, hPa	HALOE	Type = 1, 2	Type = 1, 2, 4	Ratio
82	0.96	0.67	0.69	0.70
100	2.23	0.99	1.09	0.44
121	3.02	1.47	1.63	0.49

[a]Extinction values are in units of 10^{-3} km^{-1}.Cloud types 1, 2, and 4 are unknown cloud types, laminar cirrus, and opaque clouds. Ratios are calculated by dividing the HIRDLS type 1 and 2 averages by HALOE averages.

values for latitudes between 20°S and 20°N, and between 90 and 180°E, the range of longitude over which the most prominent cloud occurrence is located. While the averages differ by a factor of two of each other, there is less variation in the range of extinction of the HIRDLS extinction field along a line of longitude (discussed below). Since the cloud frequencies in Figures 11 and 12 are similar, with similar latitudinal widths and frequencies, we expect that the extinction fields also should be similar, if the HIRDLS extinction values are accurate, and if the two experiments are able to retrieve extinction over the 1.0×10^{-5} and 1.0×10^{-2} km^{-1} extinction range equally well.

[54] The differences in the extinction fields are likely due to differences in the retrieval characteristics of the two experiments and to difficulties in the current absolute calibration of the HIRDLS 12 μm radiance profiles. Tropical HIRDLS and HALOE aerosol and cloud extinction retrieval frequencies are presented in Figure 13. The HALOE "0–25%" curve indicates, as a function of pressure, the fraction of the time (in percent) for which the HALOE experiment successfully reports extinction, for extinctions with precisions between 0 and 25%. Similar statements apply for the other curves. Both experiments report the lowest frequencies of retrieval at the low and high pressure limits of the graph. Sulfate aerosol extinction falls off in magnitude as pressure decreases, and limb path aerosol optical depths behave similarly. Large cloud optical depths and increasing gas optical depths at pressures greater than 100 hPa limit retrievals in the lower troposphere. HALOE retrieves extinction 95% of the time with a precision better than 50% for pressure near 100 hPa, while the HIRDLS experiment retrieves extinction 70% of the time at 100 hPa. A graph (not shown) of the normalized probability distribution functions of HALOE and HIRDLS retrieved extinction at 100 hPa indicates that HALOE retrieves extinction greater than 10^{-3} km^{-1} more frequently than the HIRDLS experiment. Examination of the graph of the latitudinal variation of averaged extinction at 100 hPa, for longitudes between 80 and 180°E (see Figure 14), suggests that the HIRDLS experiment does not retrieve extinction greater than 10^{-3} km^{-1} equally well as the HALOE experiment. Though there is scatter in the HALOE curve, due to a smaller sample size than the HIRDLS experiment, the parabolic shape of the HALOE curve differs from the flattened HIRDLS curves. The differences in the HALOE and HIRDLS extinction fields are considered to be substantially different. The HIRDLS extinction values are therefore considered to be preliminary.

7. Conclusions

[55] HIRDLS radiance profiles clearly show the presence of PSCs, cirrus layers (i.e., subvisible cirrus), and opaque clouds (see Figure 1). Radiance perturbations, i.e., 100 $(R_{obs}(i) - R_{clear}(i))/R_{clear}(i)$ values, in the 12.1 μm band (HIRDLS channel 6) are typically several hundred percent

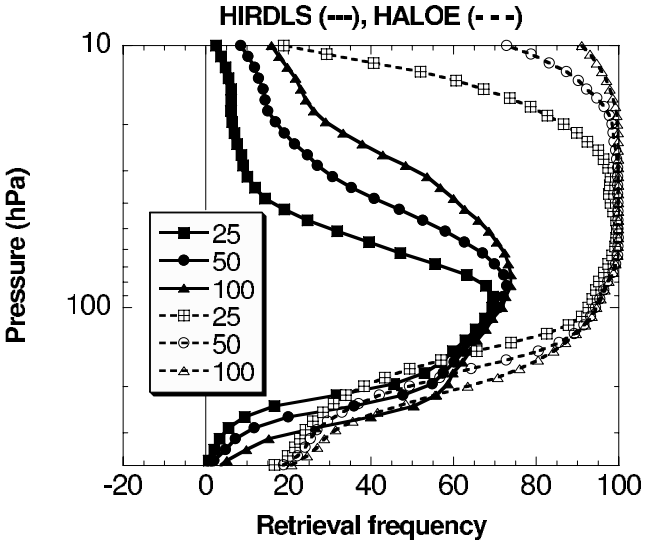

Figure 13. Retrieval frequencies of HIRDLS 12.1 μm and HALOE 3.46 μm extinction. The HIRDLS (solid line) and HALOE (dashed line) curves are for cases in which the retrieval precision is in the ranges 0–25, 0–50, and 0–100% during 2005–2006 for latitudes between 30°S and 30°N.

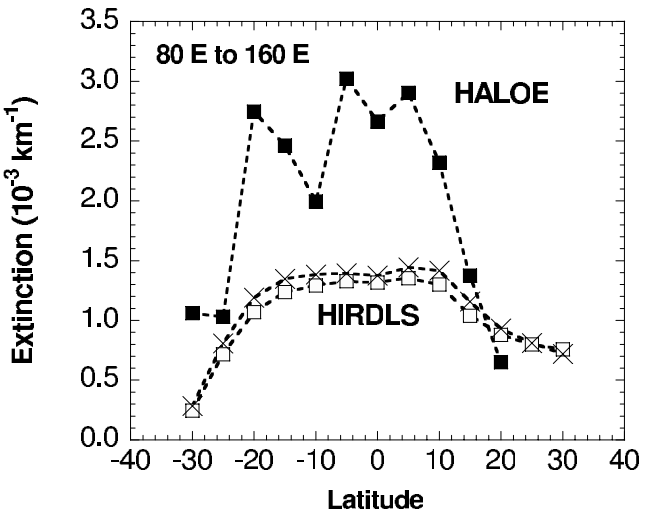

Figure 14. Comparison of HALOE and HIRDLS cloud extinctions at 100 hPa for longitudes between 80 and 180°E. HALOE data are from 1998 to 2005, while the HIRDLS data are from 2005 to 2007. Crosses correspond to cirrus layer, unknown, and opaque cloud HIRDLs extinction data, while the open squares correspond to cirrus layer and unknown cloud extinctions.

in magnitude for PSCs, cirrus layers (see Figure 2c), and opaque clouds. HIRDLS makes a full observation sequence in 10 s, measuring ~5500 profiles per day, and thus can quickly accumulate meaningful cloud statistics. As illustrated in Figures 6 and 8, HIRDLS makes many observations of PSCs and cirrus layers each day.

[56] The distributions of time averaged cloud statistics, as determined by the cloud detection algorithm, compare very well to distributions derived from correlative data. HALOE and HIRDLS time averaged cloud top pressures have a correlation coefficient of 0.87 and 0.93 in the tropics and midlatitudes, respectively (Figure 4). SAGE III and HIRDLS cloud top pressure values in 2005 have a correlation coefficient of 0.85 when the distance between observations is less than 100 km and the time difference is less than 6 h (Figure 5). Time series of the T< 195 K hemispherical area, on the 450 K potential temperature surface, and the total number of PSCs observed by the HIRDLS experiment in January and February 2005 have a correlation coefficient of 0.92 (Figure 6). CALIPSO and HIRDLS histograms of the horizontal scales of laminar cirrus in the tropics have a correlation coefficient of 0.99, though for a small sample size of five data points (Figure 10). Finally, HALOE and HIRDLS normalized distributions of cloud counts, expressed as a function of OLR, have a correlation coefficient of 0.99 (Figure 9).

[57] As discussed by *Thomason et al.* [2007], the transitory nature of clouds, and the space and time separations of different satellite orbits, makes for a difficult comparison of cloud data from two different satellite platforms. The transitory nature of clouds indeed prompted the placement of the CALIPSO and CLOUDSAT into orbital alignments that differ by 10 s in time. The sensitivity of the absolute values of cloud statistic correlation coefficients, due to the space and time differences of two different satellite experiments, is illustrated by the data presented in Table 1.The correlation coefficient of SAGE III and HIRDLS cloud top pressures is 0.45 for 531 data points separated by 0–400 km and time differences less than 24 h. The correlation coefficient becomes 0.85 for 32 data points separated by 0–400 km and time differences less than 6 h. The coefficients in Table 1 suggest that the HIRDLS cloud top pressures would correlate to SAGE III values with a correlation coefficient better than 0.85 if the space and time differences were decreased further.

[58] Tropical averages of cloud frequencies in the upper troposphere compare well to those of the HALOE experiment at 82 and 100 hPa. HALOE frequencies were determined by an analysis of multispectral HALOE extinctions, while the HIRDLS frequencies were determined by the HIRDLS cloud detection algorithm. Zonal averages of cloud frequencies at 82 and 100 hPa are within 25% of each other (Table 2), and the latitude-longitude contour maps are similar (Figures 11 and 12).

[59] Tropical averages of extinction from 1998–2005 HALOE and 2005–2007 HIRDLS extinction measurements differ by a factor of two (Table 3). Figure 13 indicates that the HIRDLS and HALOE experiments retrieve extinction 70% and 95% of the time, respectively, at 100 hPa. Normalized distributions of graphs of cloud extinction counts versus extinction indicate that the HIRDLS experiment does not retrieve extinctions larger than 10^{-3} km^{-1} as well as the HALOE experiment. HALOE and HIRDLS zonal averages of tropical extinction over the maritime continent at 100 hPa (Figure 14) differ substantially, in that the HALOE extinction curve is parabolic in shape, while the HIRDLS curve appears truncated (flat) over the equator. The HIRDLS extinction values are therefore considered to be preliminary in accuracy.

[60] **Acknowledgments.** The work discussed in this paper is funded by NASA's AURA satellite program under contract NAS5-97046. Work at the Jet Propulsion Laboratory, California Institute of Technology, was carried out under a contract with NASA. Acknowledgment is expressed to Cora Randall and Lynn Harvey of the University of Colorado for providing IDL savesets of the SAGE III data. The National Center for Atmospheric Research is sponsored by the National Science Foundation.

References

Benson, C. M., K. Drdla, G. E. Neduluha, E. P. Shettle, J. Alfred, and K. W. Hoppel (2006), Polar stratospheric clouds in the 1998–2003 Antarctic vortex: Microphysical modeling and Polar Ozone and Aerosol Measurement (POAM) III observations, *J. Geophys. Res.*, *111*, D18206, doi:10.1029/2005JD006948.

Bevilacqua, R. E., et al. (2002), Observations and analysis of PSCs detected by POAM III during the 1999/2000 Northern Hemisphere winter, *J. Geophys. Res.*, *107*(D20), 8281, doi:10.1029/2001JD000477.

Carslaw, K. S., B. Luo, and T. Peter (1995), An analytic expression for the composition of aqueous HNO_3-H_2SO_4 stratospheric aerosols including gas phase removal of HNO_3, *Geophys. Res. Lett.*, *22*(14), 1877–1880.

Edwards, D., J. C. Gille, P. L. Bailey, and J. C. Barnett (1995), Selection of sounding channels for the HIGH Resolution Dynamics Limb Sounder, *Appl. Opt.*, *34*, 7006–7018.

Hansen, J., et al. (2002), Climate forcings in Goddard Institute for Space Studies SI2000 simulations, *J. Geophys. Res.*, *107*(D18), 4347, doi:10.1029/2001JD001143.

Hervig, M., and M. McHugh (1999), Cirrus detection using HALOE measurements, *Geophys. Res. Lett.*, *26*, 719–722.

Hervig, M., et al. (1996), Validation of aerosol measurements from the Halogen Occultation Experiment, *J. Geophys. Res.*, *101*, 10,267–10,275.

Jensen, E. J., and L. Pfister (2004), Transport and freeze-drying in the tropical tropopause layer, *J. Geophys. Res.*, *109*, D02207, doi:10.1029/2003JD004022.

Jensen, E. J., S. Kinne, and O. B. Toon (1994), Tropical cirrus cloud radiative forcing: Sensitivity studies, *Geophys. Res. Lett.*, *21*(18), 2023–2026.

Jensen, E. J., L. Pfister, A. S. Ackerman, A. Tabazadeh, and O. B. Toon (2001), A conceptual model of the dehydration of air due to freeze-drying by optically thin, laminar cirrus rising slowly across the tropical tropopause, *J. Geophys. Res.*, *106*(D15), 17,237–17,252.

Kent, G. S., K. H. Sage, C. R. Trepte, and P-.H. Wang (2007), Stratospheric Aerosol and Gas Experiment III cloud data product, *Appl. Opt.*, *46*(8), 1261–1278.

Kinnison, D. E., et al. (2007), Sensitivity of chemical tracers to meteorological parameters in the MOZART-3 chemical transport model, *J. Geophys. Res.*, *112*, D20302, doi:10.1029/2006JD007879.

Lambert, A., P. L. Bailey, D. P. Edwards, J. C. Gille, B. R. Johnson, C. M. Halvorson, S. T. Massie, and K. A. Stone (1999), High-Resolution Dynamics Limb Sounder, Level-2 Algorithm Theoretical Basis Document, Oxford Univ., Oxford, U. K. (Available at http://www.atm.ox.ac.uk/user/wells/atbd.html)

Massie, S. T., et al. (1994), Spectral signatures of polar stratospheric clouds and sulfate aerosol, *J. Atmos. Sci.*, *51*(20), 3027–3044.

Massie, S. T., A. Gettelman, W. Randel, and D. Baumgardner (2002), Distribution of tropical cirrus in relation to convection, *J. Geophys. Res.*, *107*(D21), 4591, doi:10.1029/2001JD001293.

McCormick, M. P., and R. E. Veiga (1992), SAGE II measurements of early Pinatubo aerosols, *Geophys. Res. Lett.*, *19*, 155–158.

McCormick, M. P., H. M. Steele, P. Hamill, W. P. Chu, and T. J. Swissler (1982), Polar stratospheric cloud sightings by SAM II, *J. Atmos. Sci.*, *39*, 1387–1397.

Mergenthaler, J. L., A. E. Roche, J. B. Kumer, and G. A. Ely (1999), Cryogenic Limb Array Etalon Spectrometer observations of tropical cirrus, *J. Geophys. Res.*, *104*(D18), 22,183–22,194.

Pfister, L., et al. (2001), Aircraft observations of thin cirrus clouds near the tropical tropopause, *J. Geophys. Res.*, *106*, 9765–9786.

Poole, L. R., and M. C. Pitts (1994), Polar stratospheric cloud climatology based on Stratospheric Aerosol Measurement II observations from 1978 to 1989, *J. Geophys. Res.*, *99*, 13,083–13,089.

Roche, A. E., et al. (1993), The Cryogenic Limb Array Etalon Spectrometer (CLAES) on UARS: Experiment description and performance, *J. Geophys. Res.*, *98*(D6), 10,763–10,775.

Rodgers, C. D. (2000), *Inverse Methods for Atmospheric Sounding, Theory and Practice*, World Sci., Hackensack, N. J.

Russell, J., et al. (1993), The Halogen Occultation Experiment, *J. Geophys. Res.*, *98*, 10,777–10,797.

Saitoh, N., S. Hayashida, Y. Sasano, and L. L. Pan (2002), Characteristics of Arctic polar stratospheric clouds in the winter of 1996/1997 inferred from ILAS measurements, *J. Geophys. Res.*, *107*(D24), 8205, doi:10.1029/2001JD000595.

Santer, B. D., et al. (2003), Behavior of tropopause height and atmospheric temperature in models, reanalyses, and observations: Decadal changes, *J. Geophys. Res.*, *108*(D1), 4002, doi:10.1029/2002JD002258.

Spang, R., J. J. Remedios, L. J. Kramer, L. R. Poole, M. D. Fromm, M. Muller, G. Baumgarten, and P. Konopka (2005), Polar stratospheric cloud observations by MIPAS on ENVISAT: detection method, validation and analysis of northern hemisphere winter 2002/2003, *Atmos. Chem. Phys.*, *5*, 679–692.

Tabazadeh, A., R. P. Turco, and M. Z. Jacobson (1994), A model for studying the composition and chemical effects of stratospheric aerosols, *J. Geophys. Res.*, *99*(D6), 12,897–12,914.

Taylor, F. W., et al. (1993), Remote sensing of atmospheric structure and composition by pressure modulator radiometry from space: The ISAMS experiment on UARS, *J. Geophys. Res.*, *98*(D6), 10,799–10,814.

Taylor, F. W., A. Lambert, R. G. Grainger, C. D. Rogers, and J. J. Remedios (1994), Properties of Northern Hemisphere polar stratospheric clouds and volcanic aerosol in 1991/92 from UARS/ISAMS satellite measurements, *J. Atmos. Sci.*, *51*, 3019–3026.

Thomason, L. W., L. R. Poole, and C. E. Randall (2007), SAGE III aerosol extinction validation in the Arctic winter: Comparisons with SAGE II and POAM III, *Atmos. Chem. Phys.*, *7*, 1423–1433.

Wang, P. H., et al. (1996), A 6-year climatology of cloud occurrence frequency from Stratospheric Aerosol and Gas Experiment II observations (1985–1990), *J. Geophys. Res.*, *101*(D23), 29,407–29,429.

Winker, D. M., and C. R. Trepte (1998), Laminar cirrus observed near the tropical tropoause by LITE, *Geophys. Res., Lett.*, *25*(17), 3351–3354.

World Meteorological Organization (1999), Lower stratospheric processes, in *Scientific Assessment of Ozone Depletion: 1998*, chap. 7, pp. 7.1–7.6, Geneva, Switzerland.

J. Barnett and C. Hepplewhite, Department of Physics, University of Oxford, Oxford OX1 3PU, UK.

C. Cavanaugh, M. Coffey, C. Craig, T. Eden, G. Francis, J. Gille, C. Halvorson, R. Khosravi, D. Kinnison, H. Lee, S. Massie, B. Nardi, and D. Packman, National Center for Atmospheric Research, Boulder, CO 80307, USA. (massie@ucar.edu)

J. Craft, V. Dean, and D. Ellis, Center for Limb Atmospheric Sounding, University of Colorado, Boulder, CO 80309, USA.

A. Lambert and G. Manney, Jet Propulsion Laboratory, California Institute of Technology, Pasadena, CA 91109, USA.

M. Legg, Bay Area Environmental Research Institute, Sonoma, CA 95476, USA.

A. Strawa, NASA Ames Research Center, Moffett Field, CA 94035, USA.